International Journal of Computer Information Systems and Industrial Management Applications
ISSN 2150-7988 Volume 18(12s) 2026 pp. 895-898
https://doi.org/10.70917/ijcisim-2026-3961
Article

Partial substitution of cobalt with nickel on $LaCoO_3$: Structural and morphological properties

D. Mejía[1], V. Isaza-Zapata[1], J. Doria[1] and J.L. Izquierdo[1*]

[1]Institución Universitaria Pascual Bravo, Facultad de Ingeniería, Grupo de Investigación e Innovación en Energía GIIEN, CP 050001, Medellín, Colombia
*Corresponding author: jorge.izquierdo@pascualbravo.edu.co

Abstract. We present and discuss the results obtained for the 10% Ni-doped $LaCoO_3$ sample, synthesized by solid-state reaction. Through the experimental technique, x – ray diffraction, the sample was analyzed and Rietveld refinement of the XRD data was used for crystal structural determination, the results found in this process verified a single phase of $LaCo_{0.9}Ni_{0.1}O_3$ with rhombohedral crystal structure (space group $R\bar{3}c$: R). In turn, the sample was also investigated with Raman spectroscopy at room temperature to identify the characteristic Raman peaks of the phase. The morphologic properties of the sample were analyzed using Scanning Electron Micrograph and Transmission Electron Micrograph.
Keywords: Lanthanum cobaltite, Structure, Rietveld, Raman spectroscopy.

1. Introduction

The substitution of transition metals in perovskite-type oxides such as $LaCoO_3$, offers a pathway to evaluate their structural and functional properties for various technological applications; such as, thermoelectric generators [1, 2], for the use of renewable energies [3-5], and for the recovery of waste heat [6, 7]. Several researchers studied the substitution of trivalent ion, Ni^{3+}, for Co^{3+} in $LaCoO_3$ [8]. The authors investigated the electrical and thermoelectric properties of $LaCo_{1-x}Ni_xO_3$ ($0 \leq x \leq 0.2$) and found that substituting Co^{3+} with Ni^{3+} significantly enhances electrical conductivity, though it leads to a reduction in the Seebeck coefficient [8]. In addition to the substitution of Co^{3+} by Ni^{3+}, the substitution of La^{3+} by divalent ion in $LaCoO_3$, such as Ca^{2+}, Sr^{2+}, Ba^{2+} has a significant influence on the oxygen vacancy concentration and crystal-structure distortions, which also affect the physical properties [9, 10]. The thermoelectric efficiency of a material is largely determined by its chemical composition, crystal structure, and morphology [11]. However, the literature contains fewer earlier reports about the influence of Co^{3+} substitution with Ni^{2+} ions on its crystal structure, vibrational modes, and morphological features.

In this work, we report on the synthesis and characterization of a 10% Ni-doped $LaCoO_3$ ($LaCo_{0.9}Ni_{0.1}O_3$) compound prepared by solid-state reaction, with emphasis on its crystal structure, vibrational modes, and morphological features.

2. Materials and Methods

The polycrystalline $LaCo_{0.9}Ni_{0.1}O_3$ sample was prepared by means of standard solid-state reaction. High-purity stoichiometric quantities of La_2O_3, NiO, and Co_3O_4 were thoroughly mixed and ground in an agate mortar. The resulting mixture was then gradually heated in air to 1573 K and maintained for 30 hours. The overall reaction is represented by the following equation:

$$La_2O_3 + \frac{2}{3}(1-x)Co_3O_4 + 2(x)NiO \rightarrow 2LaCo_{(1-x)}Ni_xO_3 + xO_2 \uparrow$$

The reacted powders were pressed and sintered in air at 1573 K for 48 hours. After sintering, the samples were cooled to room temperature in the furnace. The crystal structure of the sintered pellets was characterized by X-ray diffraction (XRD) using a Bruker D8 Advance Eco diffractometer with CuKα radiation (λ = 1.5406 Å) in the standard θ–2θ configuration. Crystallographic parameters, including unit cell dimensions, were determined through Rietveld refinement using the MAUD software. Furthermore, the microstructure of the samples was

examined using a Scanning Electron Microscope (JEOL-JSM 6490LV) and Transmission Electron Microscopy (TEM). Phase purity was additionally assessed using Raman spectroscopy.

3. Results and discussion

3.1 Morphological and structural properties

Figure 1(a) reveals the SEM micrographs of sintered powders for the $LaCo_{0.9}Ni_{0.1}O_3$ sample. It can be observed that the morphology is not very porous, with agglomerated particles forming clusters composed of grains ranging between 3 and 3.5 µm. The chemical composition of the samples is shown in the EDS spectra (figure 1 (b)). The absence of foreign elements in the analyzed samples confirms their compositional purity.

Figure 2 shows TEM images of the sintered powders. The low-magnification image in Fig. 2(a) reveals the morphology of individual crystallites with approximate sizes of ~60 nm, while the high-resolution image in Fig. 2(b) displays lattice fringes of crystallites with varying orientations.

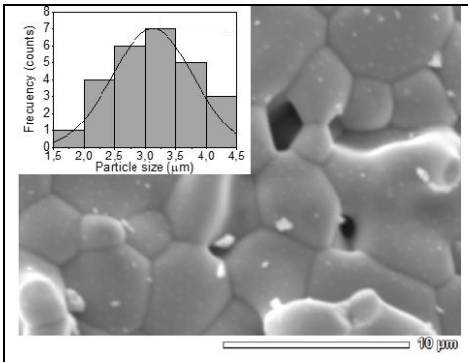

Figure 1 (a)

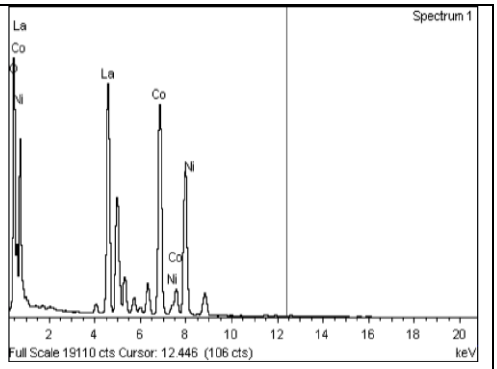

Figure 1 (b)

Figure 1. SEM micrograph for the $LaCo_{0.9}Ni_{0.1}O_3$ sample (a) and EDS (b).

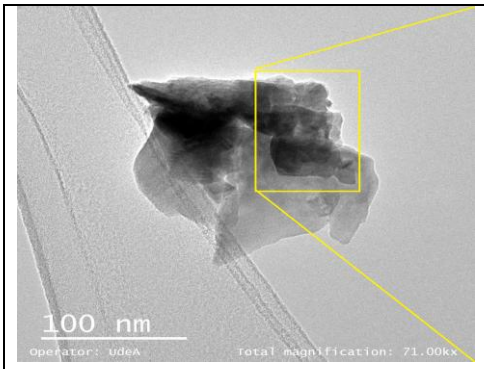

Figure 2 (a)

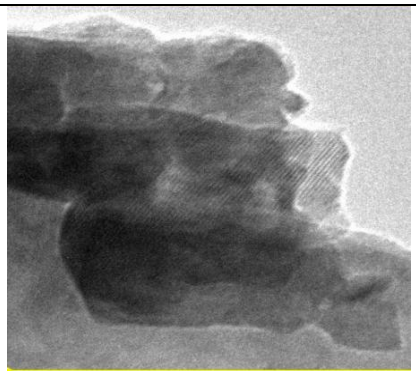

Figure 2 (b)

Figure 2. TEM micrograph for the $LaCo_{0.9}Ni_{0.1}O_3$ sample (a) high-resolution image (b).

Figure 3 displays the XRD pattern of the $LaCo_{0.9}Ni_{0.1}O_3$ sample along with their corresponding Rietveld refinements. The diffraction data were refined using the α-$LaCoO_3$ crystal structure (PDF-1530874) [12], confirming the formation of a single-phase $LaCo_{0.9}Ni_{0.1}O_3$, exhibiting a rhombohedral crystal structure (space group $R\bar{3}c$: R), and lattice parameters of a = 5.3416(2) Å and α = 60.7909 (2)° at room temperature. These findings are consistent with previously reported data for polycrystalline $LaCoO_3$ materials [12].

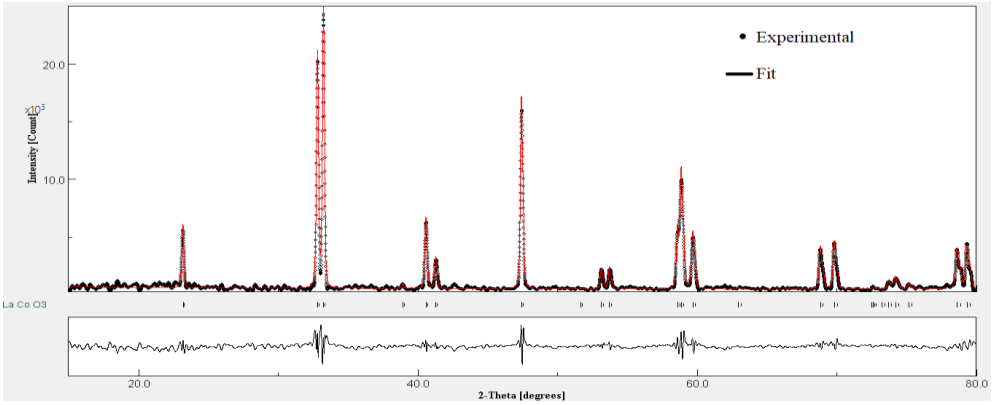

Figure 3. X-ray diffraction pattern of $LaCo_{0.9}Ni_{0.1}O_3$ bulk samples.

The solid line indicates the Rietveld pattern. Bragg reflections are indicated by tick marks. The difference between measured and calculated profiles is shown as a curve at the bottom of the diagram.

3.2 Raman spectroscopy

The phase purity of the sample was evaluated using Raman spectroscopy. The $LaCo_{0.9}Ni_{0.1}O_3$ cobaltite was characterized with a DXR3 Raman Spectrometer equipped with 532 nm and 785 nm excitation lasers. The room-temperature spectrum (Figure 4) shows six vibrational modes at 147.6, 181.2, 473.3, 518.7, 611.6, and 679.5 cm^{-1}, consistent with the characteristic Raman modes of $LaCoO_3$.

The band at ~ 147 cm^{-1} is associated with E_g La stretching vibration, while that at ~ 679 cm^{-1} is Raman-inactive for rhombohedral perovskites, show high scattering intensity due to strong electron–phonon interactions [13]. The band at 518,6 and 611,6 cm^{-1} can be related to the E_g bending vibrations in the non-JT distorted phase [14]. The two modes at ~520 and ~ 611 cm^{-1}. This bands can be assigned to the bending-type vibrations of A_g and B_g symmetry in the JT distorted phase. Based on the reported phonon energies on rhombohedrally distorted perovskite [15, 16], the mode 181,2 cm^{-1} can be assigned to the E_g vibrational mode of La atoms along the *a* and *b* axes,

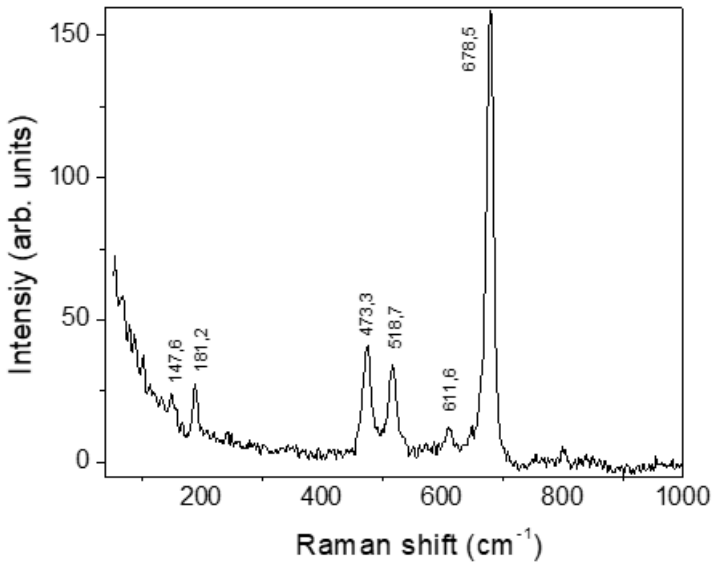

Figura 4. Modos de vibración para la muestra $LaCo_{0.9}Ni_{0.1}O_3$

4. Conclusions

In this work, a 10% Ni-doped $LaCoO_3$ cobaltite ($LaCo_{0.9}Ni_{0.1}O_3$) was successfully synthesized by solid-state reaction and characterized to evaluate the influence of Ni substitution on its structural, vibrational, and morphological properties. XRD analysis followed by Rietveld refinement confirmed the formation of a single-phase material with a rhombohedral crystal structure (space group $R\bar{3}c$), consistent with the reported structure of undoped $LaCoO_3$. Raman spectroscopy further supported the phase purity of the sample, revealing seven vibrational modes characteristic of $LaCoO_3$. Morphological analysis by SEM and TEM showed that the material

is composed of porous agglomerates of micron-sized grains, with crystallites exhibiting well-defined lattice fringes.

These findings contribute to a deeper understanding of the structural and vibrational response of Ni-substituted cobaltites, offering valuable insights for future studies aimed at tailoring their thermoelectric and electronic properties.

Acknowledgements

J. Doria and J. L. Izquierdo acknowledge the financial support from Dirección de Ciencia, Tecnología e Innovación of the Institución Universitaria Pascual Bravo, Colombia, Medellín Campus.

References

1. X. Wen, J. Ji, Z. Song, Z. Li, Performance prediction of the concentrated hybrid power/thermal system incorporating thermoelectric generators, Appl. Therm. Eng. 212 (2022) 118594.
2. F. Tohidi, S. G. Holagh and A. Chitsaz, Thermoelectric Generators: A comprehensive review of characteristics and applications, Appl. Therm. Eng. 201 (2022)117793.
3. B. Akarsu and M. S. Genç, Optimization of electricity and hydrogen production with hybrid renewable energy systems, Fuel 324 (2022) 124465.
4. R. Hassan, B. K. Das and M. Hasan, Integrated off-grid hybrid renewable energy system optimization based on economic, environmental, and social indicators for sustainable development, Energy 250 (2022) 123823.
5. Y. Kirim, H. Sadikoglu, M. Melikoglu, Technical and economic analysis of biogas and solar photovoltaic (PV) hybrid renewable energy system for dairy cattle barns, Renew. Energ. 188 (2022) 873-889.
6. T. Ni, J. Si, X. Gong, K. Zhang, M. Pan, Thermodynamic and economic analysis of a novel cascade waste heat recovery system for solid oxide fuel cell, Energ. Convers. Manage. 259 (2022) 115562.
7. R. Hu, X. Liu, X. Zhang, L. Yang, Analysis of energy, economy, and carbon emission of nested cascade refrigeration cycle with heat recovery system, Int. J. Refrig. 136 (2022) 94-102.
8. F. Li and J.-F. Li, Effect of Ni substitution on electrical and thermoelectric properties of LaCoO3 ceramics, Ceram. Int. 37 (2011)105–110.
9. K. Muta, Y. Kobayashi, K. Asai, Magnetic, Electronic Transport, and Calorimetric Investigations of La1-xCaxCoO3 in Comparison with La1-xSrxCoO3, J. Phys. Soc. Jpn. 71 (2002) 2784-2791.
10. H. Masuda, T. Fujita, T. Miyashita, M. Soda, Y. Yasui, Y. Kobayashi, M. Sato, Transport and Magnetic Properties of R1-xAxCoO3 (R = La, Pr and Nd; A = Ba, Sr and Ca), J. Phys. Soc. Jpn. 72 (2003) 873-878.
11. Kim SI, et al. Dense dislocation arrays embedded in grain boundaries for high-performance bulk thermoelectrics. Science. 2015;348:109–114.
12. G. Thornton, B. C. Tofield A. W. Hewat, A neutron diffraction study of LaCoO3 in the temperature range 4.2 < T < 1248 K, J. Solid State Chem. 61 (1986) 301-307.
13. Hong WT, Gadre M, Lee Y et al (2013) Tuning the spin state in $LaCoO_3$ thin films for enhanced high- temperature oxygen electrocatalysis. J Phys Chem Lett 4:2493–2499.
14. Orlovskaya N, Steinmetz D, Yarmolenko S et al (2005) Detection of temperature- and stress-induced modifications of LaCoO3 by micro-Raman spectroscopy. Phys Rev B Condens Matter Mater Phys 72:1–7.
15. E. Granado et al., Phys. Rev. B 58, 11435 (1998).
16. M.V. Abrashev et al., Phys. Rev. B 59, 4146 (1999).